

Geophysical Research Letters

RESEARCH LETTER

10.1029/2018GL080125

Key Points:

- Dayside ECH waves are preferentially observed with moderate average wave strength on the prenoonside to noonside in the outer magnetosphere
- In higher latitudinal regions, dayside ECH waves have comparable occurrence rates and wave amplitude to that of the near-equatorial regions
- Although weak dayside ECH waves occur predominantly, the occurrence rates of moderate and strong dayside ECH waves are not negligible

Supporting Information:

- Supporting Information S1

Correspondence to:

X. Gu,
guxudong@whu.edu.cn

Citation:

Lou, Y., Gu, X., Summers, D., Ni, B., Liu, K., Fu, S., et al. (2018). Statistical distributions of dayside ECH waves observed by MMS. *Geophysical Research Letters*, 45, 12,730–12,738. <https://doi.org/10.1029/2018GL080125>

Received 21 AUG 2018

Accepted 29 NOV 2018

Accepted article online 3 DEC 2018

Published online 13 DEC 2018

Statistical Distributions of Dayside ECH Waves Observed by MMS

Yuequn Lou¹ , Xudong Gu¹ , Danny Summers² , Binbin Ni¹ , Kaijun Liu³ , Song Fu¹ , Zheng Xiang¹ , Zhengyang Zou¹ , Xing Cao¹ , Wenxun Zhang¹ , He Huang¹ , and Ying He¹

¹School of Electronic Information, Wuhan University, Wuhan, China, ²Department of Mathematics and Statistics, Memorial University of Newfoundland, St. John's, Newfoundland and Labrador, Canada, ³Department of Earth and Space Sciences, Southern University of Science and Technology, Shenzhen, China

Abstract Strong electrostatic electron cyclotron harmonic (ECH) waves on the dayside magnetosphere have been reported based on observations of the Magnetospheric Multiscale (MMS) spacecraft. In this study, we analyze high-quality wave data from the four MMS satellites between 1 September 2015 and 30 August 2018 to investigate the statistical properties of dayside ECH emissions. The results show that dayside ECH waves are preferentially observed on the prenoon side in the outer magnetosphere ($L = 8\text{--}12$), with average wave amplitude $E_w > 0.1 \text{ mV/m}$. In addition, besides the typical near-equatorial ($|\text{MLAT}| \leq 15^\circ$) region, dayside ECH waves exhibit moderate occurrence rate and wave amplitude in higher latitudinal regions (i.e., $15^\circ < |\text{MLAT}| \leq 40^\circ$), possibly due to the off-equatorial geomagnetic field minimum. Our reported double peaks of dayside ECH wave occurrence zone and considerable occurrence rates of prenoonside ECH waves suggest that dayside ECH waves can be a potentially important contributor to the formation of dayside diffuse aurora.

Plain Language Summary We use wave spectral data from the four Magnetospheric Multiscale (MMS) spacecraft to statistically analyze the distributions of wave amplitudes and occurrence rates as a function of L shell, MLT, geomagnetic activity (AE* and Kp indices), and MLAT for dayside first harmonic band electron cyclotron harmonic (ECH) waves. The conclusions are summarized as follows: (1) Dayside ECH waves preferentially occur on the prenoonside of the outer magnetosphere, with peak occurrence rates around 30%. (2) In higher latitudinal regions ($|\text{MLAT}| = 15\text{--}25^\circ, 25\text{--}40^\circ$), contrary to previous conclusions regarding ECH wave occurrence patterns, dayside ECH waves occur with significant occurrence rates, comparable to that of dayside ECH waves in near-equatorial areas. (3) Similar to the distribution of occurrence rates, dayside ECH waves have most intense electric field amplitudes over $L = 8\text{--}12$, $\text{MLT} = 8\text{--}11$, with an average wave strength $>0.1 \text{ mV/m}$. Whistler mode chorus waves are considered as the primary mechanism to explain dayside diffuse aurora, but the role of ECH waves has not been systematically evaluated because of lack of dayside ECH observations. As shown by our results, moderate dayside ECH waves can be observed on the prenoonside of the outer magnetosphere. This observation could be of great importance in understanding the generation of dayside diffuse aurora.

1. Introduction

Electron cyclotron harmonic (ECH) emissions are electrostatic waves generated between the harmonics of electron cyclotron frequency, with dominant wave power observed around the odd integral half harmonics of the electron cyclotron frequency ($n + 1/2$) f_{ce} (Kennel et al., 1970; Meredith et al., 2009; Ni, Thorne, Liang, et al., 2011; Ni et al., 2017; Zhang & Angelopoulos, 2014). Determined by the electrostatic nature of ECH waves, the waves propagate with very large wave normal angles, almost perpendicular to the ambient magnetic field (Gurnett & Bhattacharjee, 2005). Generally, ECH waves are believed to be excited by the loss cone instability of an ambient, hot electron velocity distribution (Ashour-Abdalla & Kennel, 1978; Horne, 1989; Horne et al., 2003).

ECH waves were first reported by Kennel et al. (1970) using OGO-5 data. The magnitudes of wave amplitudes were typically several millivolts per meter and occasionally up to 100 mV/m. However, subsequent studies (Belmont et al., 1983; Roeder & Koons, 1989) indicated that the electric field amplitudes of ECH waves are typically more modest. The waves preferentially occur over 22–06 MLT (magnetic local time), at geocentric

distances between 4 and 8, near the magnetic equator. Meredith et al. (2009) revealed the strong dependence of the intensity of ECH waves on geomagnetic conditions by using higher-resolution data from CRRES. However, these data only cover the spatial region $L < 7$, and there is a lack of observations on the prenoonside for $L > 5$ due to orbital restrictions. Later statistical analyses (Ni, Thorne, Liang, et al., 2011; Ni et al., 2017; Zhang & Angelopoulos, 2014) found that strong ECH waves can extend to $10 R_E$ in the premidnight to dawn sector, near the magnetic equator, using measurements from Time History of Events and Macroscale Interactions during Substorms.

ECH waves and whistler mode chorus are considered as the two major mechanisms for generating diffuse aurora (Horne et al., 2003; Meredith et al., 2009; Ni et al., 2008, 2014, 2016; Ni, Thorne, Meredith, et al., 2011; Ni, Thorne, Horne, et al., 2011; Ni & Thorne, 2012; Tao et al., 2011; Thorne et al., 2010). These two types of plasma wave can pitch angle scatter hundreds to several thousand electronvolts plasma sheet electrons, which are the source population for diffuse aurora (Lui et al., 1977; Meng et al., 1979), into the loss cone and cause them to precipitate into the atmosphere. For the nightside diffuse aurora, whistler mode chorus waves play the primary role in forming the most intense diffuse aurora in the inner magnetosphere for $L < 8$ (Li et al., 2009, 2011; Ni et al., 2008; Ni, Thorne, Meredith, et al., 2011; Thorne et al., 2010), while ECH waves are responsible for the diffuse aurora in the outer magnetosphere (Liang et al., 2011; Ni, Thorne, Liang, et al., 2011; Ni et al., 2012). The dayside diffuse aurora is generally weaker than that on the nightside (Newell et al., 2009) but still has considerable effect on the dayside magnetosphere-ionosphere coupling (Ni et al., 2014, 2016). The main contributor to dayside diffuse aurora is still under debate. A recent study (Ni et al., 2014) proposed that whistler mode chorus can be an efficient mechanism for generating the dayside diffuse aurora, but the efficiency of ECH waves in driving dayside diffuse aurora has not yet been systematically evaluated.

The Magnetospheric Multiscale (MMS) mission launched by NASA in 2015 has high-resolution data and the orbits cover a broad magnetic latitude range (Burch & Torbert, 2016). Dayside ECH waves have been observed by MMS (Han et al., 2017), and furthermore, the satellites focus on dayside measurements in Phase 1 of the mission. Here our study is designed to statistically analyze the occurrence rate pattern and wave amplitudes of dayside ECH waves using MMS data.

2. ECH Selection Criteria

Launched on 12 March 2015, the MMS mission consists of four identical spacecraft to understand the mechanism of magnetic reconnection on the dayside and in the magnetotail (Burch et al., 2016). The MMS mission was operated in two phases with different orbital design (Fuselier et al., 2016). During Phase 1, orbits with perigees of $1.2 R_E$ and apogees $12 R_E$ were adopted to focus on dayside magnetosphere measurements, while in Phase 2, orbits with perigees of $1.2 R_E$ and apogees of $25 R_E$ were used for nightside observations. The periods of the orbit are about 1 and 3 days, respectively. The four spacecraft, flying in a tetrahedral configuration with separation distance ranging from ~ 10 to ~ 160 km in Phase 1 have very similar results for wave observation.

In this paper, we use the electric field data from the electric field double probe (Ergun et al., 2016; Lindqvist et al., 2016) and the magnetic field data from the digital signal processor (Torbert et al., 2016). Since the payloads of the spacecraft commissioned from September 2015, and then concentrated on dayside observations, we therefore analyze the statistical properties of ECH waves using data from the four MMS spacecraft during time period between 1 September 2015 and 30 August 2018. Using high-resolution (1 min) OMNIWeb data of solar wind parameters and geomagnetic indices, the T04S magnetic field model maps the spacecraft position in geocentric solar magnetospheric (GSM) coordinates to the corresponding L shell, MLT, and magnetic latitude (λ) (Tsyganenko & Sitnov, 2005).

We select ECH events according to the following criteria:

1. Data points with the northward component of the ambient magnetic field (B_z) ≤ 10 nT or electron density $\geq 4 \text{ cm}^{-3}$ are excluded from our database to avoid events that are possibly outside the magnetopause (Case & Wild, 2013).
2. Using magnetic field data measured from the Fluxgate Magnetometer (Russell et al., 2016), we can calculate the local electron cyclotron frequency using local ambient magnetic field from satellite

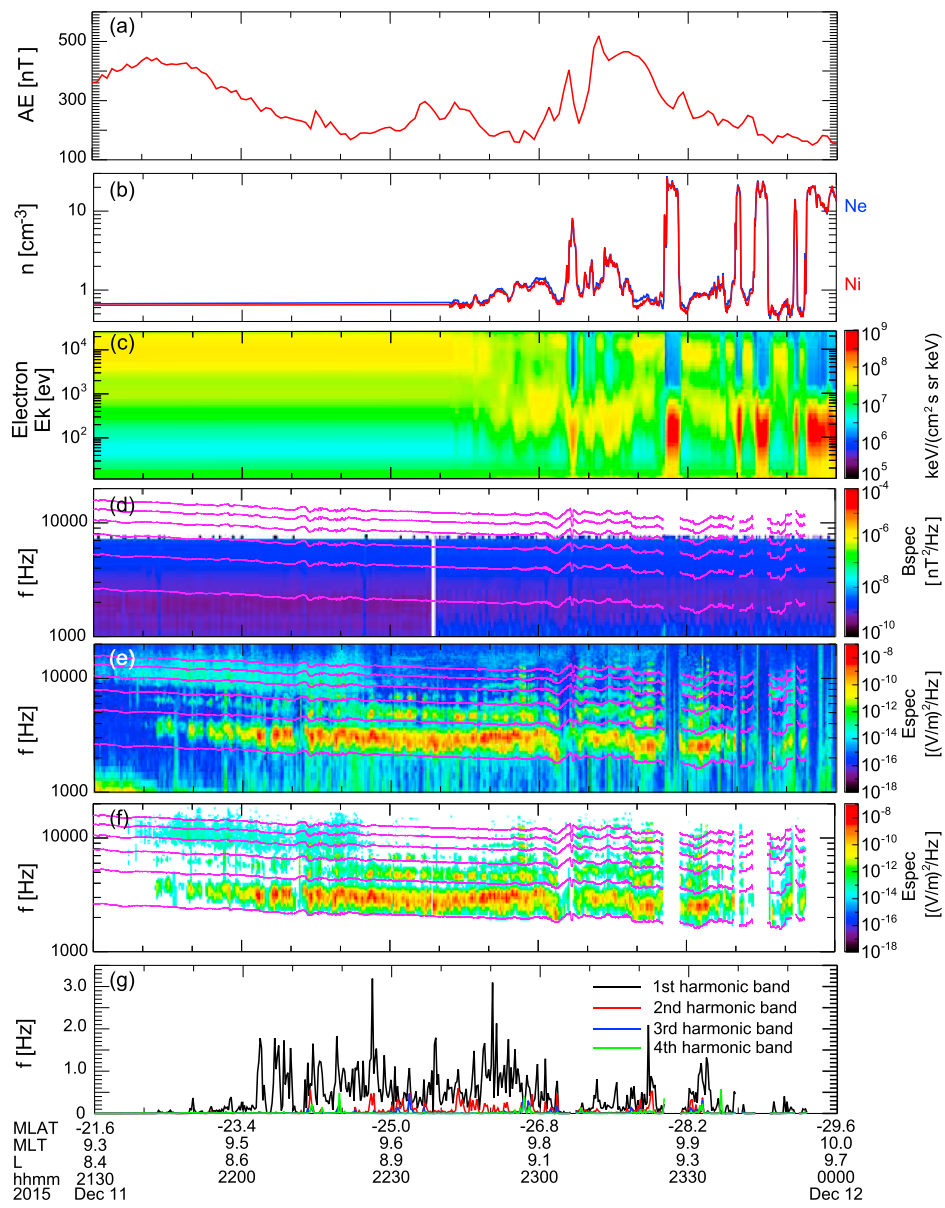


Figure 1. An example of dayside electron cyclotron harmonic wave event observed by Magnetospheric Multiscale 1 using the automatic selection criteria. From top to bottom: (a) AE index; (b) electron and ion number density; (c) electron omnidirectional flux; (d), (e) magnetic and electric field power spectral densities; (f) electric field power spectral densities for the identified electron cyclotron harmonic wave; and (g) the corresponding electric field wave amplitudes with the black, red, blue, and green lines for the first four harmonic bands, respectively. The magenta lines in panels (d)–(f) indicate f_{ce} , $2f_{ce}$, $3f_{ce}$, $4f_{ce}$, $5f_{ce}$, and $6f_{ce}$, respectively.

- measurements to help us identify the ECH events. Moreover, since the first harmonic band is predominant in ECH emissions, we only discuss the distribution of the first harmonic band dayside ECH waves.
3. The wave amplitude is calculated by integrating the power spectrum density over a specified frequency range. Owing to the electrostatic nature of ECH waves and the instrument noise, we limit the magnetic field amplitude <4 pT and electric field amplitude ≥ 0.01 mV/m.
 4. To eliminate the impact of broadband electrostatic noises, we only adopt data points with the ratio of peak wave intensity between f_{ce} – $2f_{ce}$ and wave intensity at f_{ce} above 5.

With these criteria, we establish a database of ECH emissions for subsequent detailed analysis. An example ECH event using the above criteria is shown in Figure 1. Figure 1a shows the AE index. Figure 1b shows the electron and ion number density. Figure 1c shows the electron omnidirectional flux. These two

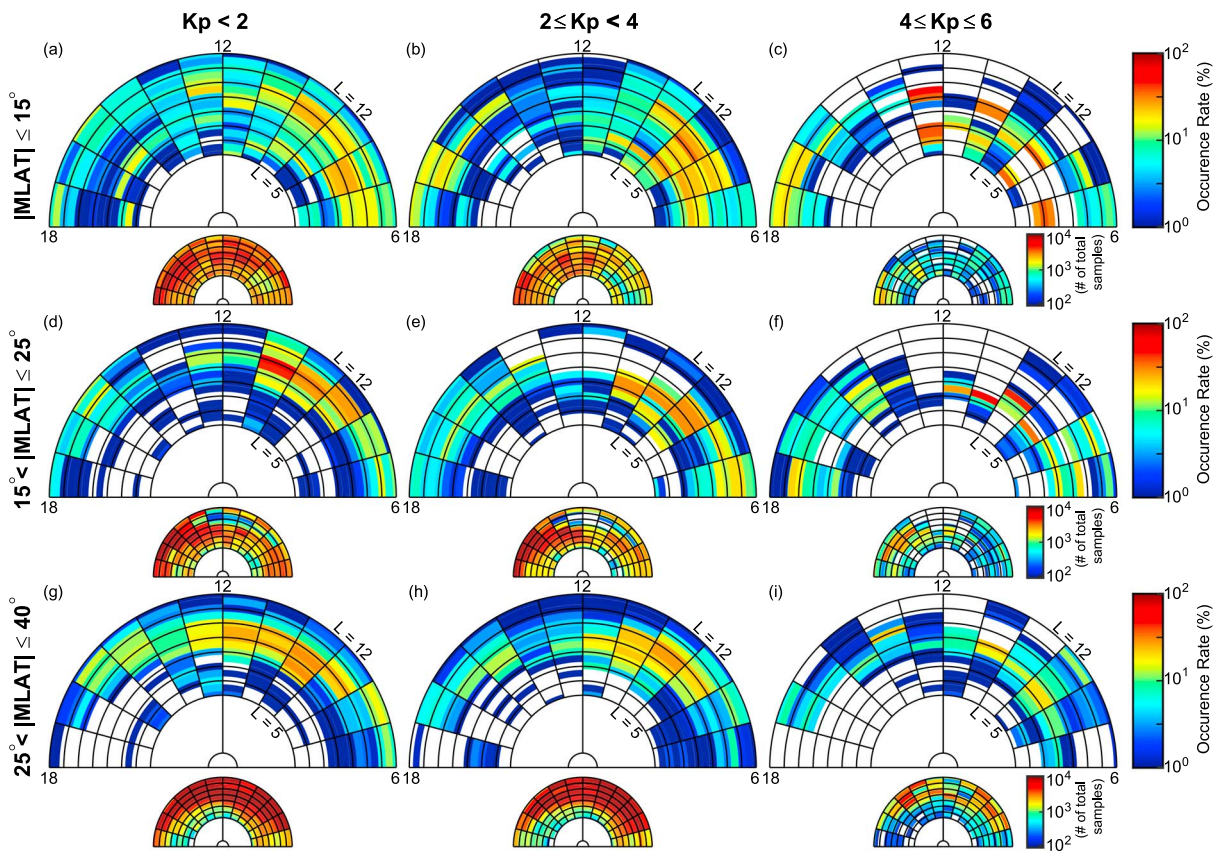


Figure 2. Statistical occurrence rates of dayside electron cyclotron harmonic waves as a function of L shell and magnetic local time for the three indicated geomagnetic conditions (from left to right: $Kp < 2$, $2 \leq Kp < 4$, and $4 \leq Kp \leq 6$) in the (a–c) near-equatorial ($|MLAT| \leq 15^\circ$), (d–f) midlatitude ($15^\circ < |MLAT| \leq 25^\circ$), and (g–i) high-latitude regions ($25^\circ < |MLAT| \leq 40^\circ$). The larger plots show the occurrence rates of dayside electron cyclotron harmonic waves and the smaller plots the total number of satellite observation points in each bin. MLAT = magnetic latitude.

subfigures exhibit the position of spacecraft relative to the magnetopause (Li et al., 2018; Wilder et al., 2016). Figures 1d and 1e show the magnetic and electric field power spectral densities, respectively. In Figure 1f, the power spectral density under 10^{-14} (V/m) 2 /Hz is left blank, and we can see that the ECH emission has mostly been preserved. Figure 1g shows the wave amplitudes of the first four harmonic bands. The magenta lines in the figure from bottom to the top indicate f_{ce} , $2f_{ce}$, $3f_{ce}$, $4f_{ce}$, $5f_{ce}$, and $6f_{ce}$, respectively.

3. Statistical Results

Figure 2 shows the occurrence rates and number of total samples as a function of L shell and MLT for different geomagnetic conditions and magnetic latitudes. For each of the three magnetic latitude intervals (near-equatorial: $|MLAT| \leq 15^\circ$, midlatitude: $15^\circ < |MLAT| \leq 25^\circ$, and high-latitude: $25^\circ < |MLAT| \leq 40^\circ$), we consider the three geomagnetic conditions ($Kp < 2$, $2 \leq Kp < 4$, and $4 \leq Kp \leq 6$). In this figure, the regions of our interest ($MLT = 6\text{--}18$, L shell = 5–12) have been divided into smaller bins with the resolution $0.5 L \times 1$ MLT. The smaller panels represent the sample number of MMS observations in each bin, while the larger panels display the corresponding occurrence rates of dayside ECH emissions. The latter denote the ratio of ECH wave observations to the sample numbers, where the ECH wave observations are obtained by using our automatic criteria. In a given bin, if there are no data that satisfy the criteria, the corresponding region in the figure is left blank. From the figure, we can see that the peak occurrence rate regions of dayside ECH waves are located on the prenoon-side in the outer magnetosphere, for all relevant geomagnetic conditions and magnetic latitude intervals. For $|MLAT| \leq 15^\circ$, as the Kp index rises, the peak occurrence rates of dayside ECH waves increase generally. At $Kp < 4$, the maximum of occurrence rates (~30%) occurs at $L = 7\text{--}10$ and $MLT = 7\text{--}9$. At $4 \leq Kp \leq 6$, the maximum of occurrence rates is >50%, while the number of samples is not abundant enough for statistical analysis, thus decreasing the reliability of this result. For $15^\circ < |MLAT| \leq 25^\circ$, compared with the near-equatorial

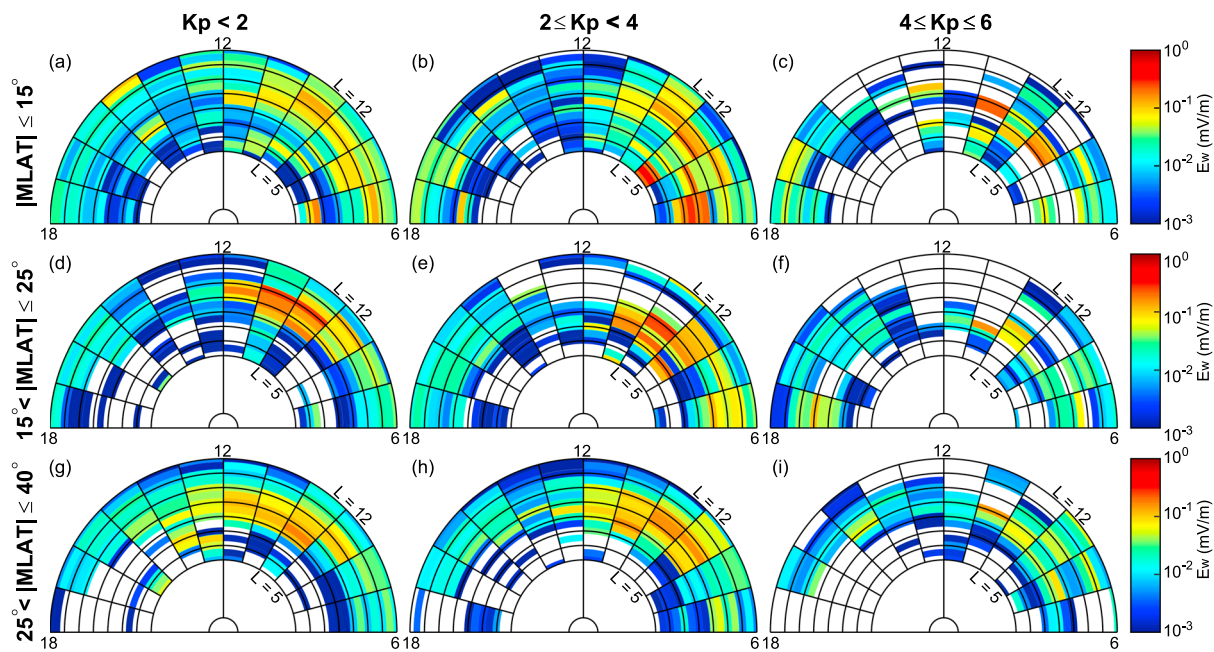


Figure 3. Statistical distributions of average electric field wave amplitude of dayside electron cyclotron harmonic waves as a function of L shell and magnetic local time for the three indicated geomagnetic conditions (from left to right: $Kp < 2$, $2 \leq Kp < 4$, and $4 \leq Kp \leq 6$) in the (a–c) near-equatorial ($|MLAT| \leq 15^\circ$), (d–f) midlatitude ($15^\circ < |MLAT| \leq 25^\circ$), and (g–i) high-latitude ($25^\circ < |MLAT| \leq 40^\circ$) regions.

region, the occurrence rate of dayside ECH waves tends to increase for the cases of $Kp < 2$ and $2 \leq Kp < 4$ with the peak occurrence rate region shifting to higher L shells closer to the noon side. As the Kp index increases, dayside ECH waves are likely to occur at lower L shells, possibly because the solar wind compresses the magnetosphere closer to Earth under such conditions. For $25^\circ < |MLAT| \leq 40^\circ$, the occurrence rates are comparable to those of near-equatorial regions ($|MLAT| \leq 15^\circ$) for $Kp < 4$, but drop subsequently for $4 \leq Kp \leq 6$. The high occurrence rates at high latitudes may be caused by the presence of off-equatorial magnetic field minimum (Shabansky, 1971), where waves can be excited more easily in both Northern and Southern Hemispheres (Ashour-Abdalla & Kennel, 1978; Horne et al., 2003; Ni, Thorne, Horne, et al., 2011).

Figure 3 displays average root-mean-square (RMS) electric field amplitude distributions of dayside ECH waves for the indicated three geomagnetic conditions and three magnetic latitude intervals, as a function of L shell and MLT. We can see from the figure that average electric field wave amplitudes of dayside ECH waves are most intense (>0.1 mV/m) on the prenoonside of the outer magnetosphere, which is similar to the occurrence pattern in Figure 2. For the near-equatorial regions, as the geomagnetic activity intensifies for $Kp < 4$, the average wave amplitudes of dayside ECH waves intensify correspondingly with the peak average wave intensity increasing from 0.22 mV/m at $Kp < 2$ to 0.45 mV/m at $2 \leq Kp < 4$. In contrast, for the case of $4 \leq Kp \leq 6$, the average wave amplitudes decrease slightly. For the midlatitude regions, as the Kp index rises, dayside ECH waves become enhanced substantially on the postnoonside but tend to first increase generally with increasing Kp index for $Kp < 4$ and subsequently decrease for $4 \leq Kp \leq 6$ on the prenoonside. For the high-latitude regions, average wave amplitudes of dayside ECH waves are generally about 0.1 mV/m at $L = 8\text{--}10$ and $MLT = 8\text{--}12$ at $Kp < 2$, and increase to approximately 0.2 mV/m with narrower spatial coverage at $2 \leq Kp < 4$. Similarly, dayside ECH waves weaken at $4 \leq Kp \leq 6$.

In Figure 4, the electric field amplitudes are sorted into three categories: relatively weak (0.01–0.1 mV/m), moderate (0.1–0.3 mV/m), and strong (>0.3 mV/m) to evaluate the global occurrence pattern of dayside ECH waves. The occurrence rate is defined as the ratio of the number of ECH samples, whose corresponding electric field amplitudes are located in the designated level of wave amplitude, to the total number of satellite observation points in each bin. Figure 4 shows the dayside occurrence pattern of different levels of ECH wave amplitude as a function of L shell and MLT at various magnetic latitudes. From Figure 4, we can see that the occurrence rates of weak (0.01–0.1 mV/m) dayside ECH waves are predominant in the observations (~25%) on the prenoonside of the outer magnetosphere. However, the occurrence rates of modest (0.1–0.3 mV/m)

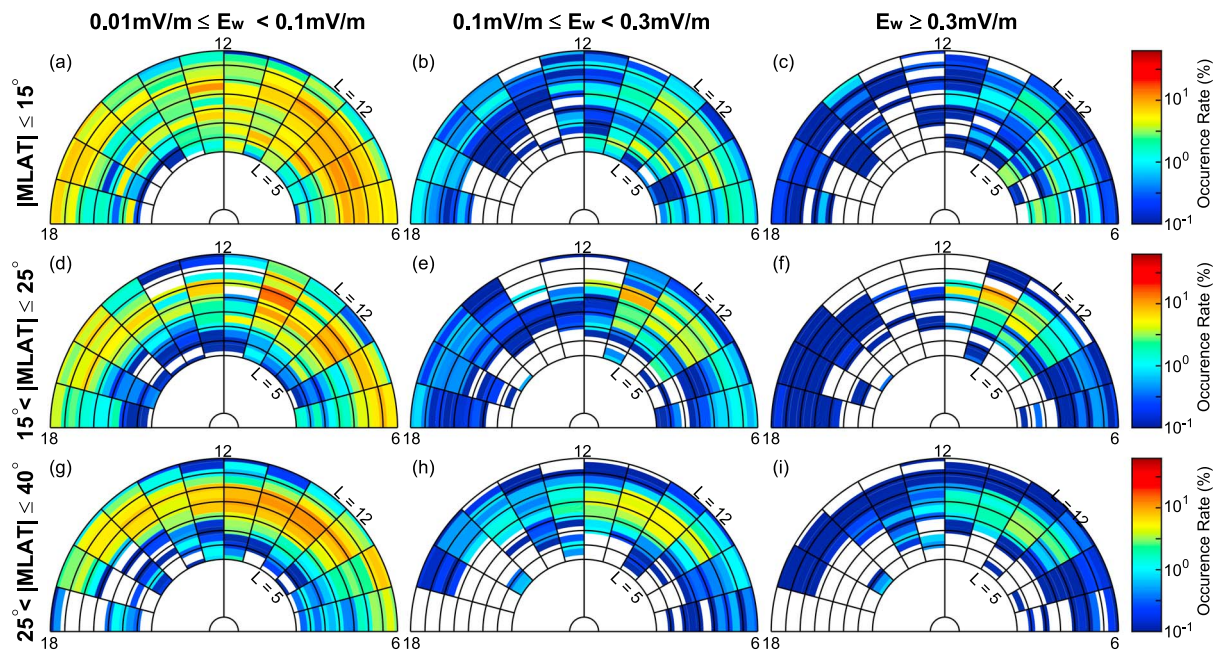


Figure 4. Statistical occurrence rates of dayside electron cyclotron harmonic waves as a function of L shell and magnetic local time in three magnetic latitude intervals and for three wave amplitude levels (from left to right: relatively weak with $0.01 \text{ mV/m} \leq E_w < 0.1 \text{ mV/m}$, moderate with $0.1 \text{ mV/m} \leq E_w < 0.3 \text{ mV/m}$, and strong with $E_w \geq 0.3 \text{ mV/m}$, respectively).

and strong ($>0.3 \text{ mV/m}$) dayside ECH waves cannot be overlooked, with the peak occurrence rates on the prenoonside of the outer magnetosphere generally at $\sim 8\%$ and $\sim 6\%$, respectively. Furthermore, as the wave strength increases, the asymmetry of occurrence rates on the prenoonside and postnoonside becomes more obvious. We can see from Figure 4 that in addition to the near-equatorial region, the high latitudinal region is another favorable zone for the occurrence of dayside ECH waves.

Table 1 exhibits the statistical average values of dayside ECH wave amplitude and peak wave frequency for two different L shell ranges (i.e., $5 \leq L \leq 8$ and $8 < L \leq 12$) in three MLT sectors (i.e., 6–10, 10–14, and 14–18) and

Table 1

Average Values of Wave Amplitude and Peak Wave Frequency of First-Band Dayside ECH Waves for Two Different L Shell Ranges in Three MLT Sectors, Three Magnetic Latitude Intervals Under Three Geomagnetic Conditions

L shell	MLT	MLAT($^\circ$)	E_w (mV/m)			f_m/f_{ce}		
			Kp < 2	2 \leq Kp < 4	4 \leq Kp \leq 6	Kp < 2	2 \leq Kp < 4	4 \leq Kp \leq 6
$5 \leq L \leq 8$	06–10	$ \text{MLAT} \leq 15$	0.062	0.166	0.063	1.61	1.59	1.36
		$15 < \text{MLAT} \leq 25$	0.007	0.115	0.038	1.60	1.43	1.46
		$25 < \text{MLAT} \leq 40$	0.013	0.030	0.011	1.48	1.47	1.35
	10–14	$ \text{MLAT} \leq 15$	0.020	0.016	0.031	1.61	1.61	1.64
		$15 < \text{MLAT} \leq 25$	0.009	0.046	0.039	1.54	1.61	1.43
		$25 < \text{MLAT} \leq 40$	0.031	0.048	0.004	1.60	1.55	1.60
	14–18	$ \text{MLAT} \leq 15$	0.009	0.002	0.001	1.51	1.61	1.27
		$15 < \text{MLAT} \leq 25$	0.006	0.001	0.020	1.44	1.31	1.39
		$25 < \text{MLAT} \leq 40$	0.015	0.001	NAN	1.73	1.51	NAN
$8 < L \leq 12$	06–10	$ \text{MLAT} \leq 15$	0.072	0.102	0.059	1.58	1.54	1.45
		$15 < \text{MLAT} \leq 25$	0.064	0.128	0.039	1.47	1.41	1.42
		$25 < \text{MLAT} \leq 40$	0.080	0.101	0.035	1.44	1.42	1.36
	10–14	$ \text{MLAT} \leq 15$	0.048	0.036	0.092	1.61	1.63	1.56
		$15 < \text{MLAT} \leq 25$	0.063	0.025	0.012	1.56	1.48	1.42
		$25 < \text{MLAT} \leq 40$	0.066	0.060	0.032	1.57	1.52	1.51
	14–18	$ \text{MLAT} \leq 15$	0.027	0.039	0.034	1.54	1.50	1.45
		$15 < \text{MLAT} \leq 25$	0.015	0.020	0.026	1.52	1.45	1.41
		$25 < \text{MLAT} \leq 40$	0.022	0.022	0.023	1.49	1.39	1.40

three geomagnetic latitude intervals (i.e., near-equatorial: $|MLAT| \leq 15^\circ$, midlatitude: $15^\circ < |MLAT| \leq 25^\circ$, and high-latitude: $25^\circ < |MLAT| \leq 40^\circ$) under three geomagnetic conditions (i.e., $K_p < 2$, $2 \leq K_p < 4$, and $4 \leq K_p < 6$), which can be readily adopted as representative inputs to quantify the electron diffusion coefficients by the first harmonic (statistically strongest) of dayside ECH waves and investigate the underlying contribution of dayside ECH emissions to the formation of dayside diffuse aurora. Overall, the average amplitude of dayside ECH waves ranges from 0.001 to 0.166 mV/m, peaking on the prenoon side at $2 \leq K_p < 4$ for $5 \leq L \leq 8$ in the near-equatorial and midlatitude regions and for $8 < L \leq 12$ in most considered latitudinal regions. In addition, the peak wave frequency is generally centralized at $1.27 f_{ce} - 1.73 f_{ce}$, and tends to decrease with increasing K_p index.

4. Conclusions and Discussions

In the present study, we have adopted the high-quality wave spectral data sets from the four MMS spacecraft to perform a statistical analysis of the distributions of wave amplitudes and occurrence rates as a function of L shell, MLT, geomagnetic latitude, and geomagnetic activity for the first harmonic band (predominantly strongest) of dayside ECH waves. Compared with previous statistical studies of ECH waves, our study mainly concentrates on the spatial distribution pattern of ECH waves on the dayside ($MLT = 6-18$) over a broad magnetic latitude range ($|MLAT| \leq 40^\circ$) in the region $L = 5-12$. Our principal conclusions are summarized as follows:

1. Dayside ECH waves are preferentially observed on the prenoon side of the outer magnetosphere, with a peak occurrence rate around 30%. The global occurrence rates of dayside ECH waves have strong L shell dependence and pronounced MLT asymmetry with respect to the prenoon side and postnoon side. As the geomagnetic latitude increases, the preferential occurrence region of dayside ECH waves tends to switch closer to the noon side. Furthermore, dayside ECH waves have an overall shift to lower L shells during geomagnetically active periods, possibly due to the solar wind compression of the magnetosphere in association with the intensification of geomagnetic activity.
2. In higher latitudinal regions (i.e., $15^\circ < |MLAT| \leq 25^\circ$, and $25^\circ < |MLAT| \leq 40^\circ$), contrary to previous studies regarding the ECH wave occurrence pattern, dayside ECH waves are observed with considerable occurrence rates, peaking at $\sim 30\%$, comparable to those of dayside ECH waves in the near-equatorial region (i.e., $|MLAT| \leq 15^\circ$). It is suggested that the presence of high-latitude dayside ECH waves is possibly a result of the off-equatorial geomagnetic field minimum where ECH waves can be more likely to generate (Ashour-Abdalla & Kennel, 1978; Horne et al., 2003; Ni, Thorne, Horne, et al., 2011).
3. Similar to the distribution of occurrence rates, dayside ECH waves are most intense over $L = 8-12$ on the prenoon side with peak average wave strength typically greater than 0.2 mV/m at $K_p < 4$. The average wave amplitudes of ECH waves in midlatitude ($15^\circ < |MLAT| \leq 25^\circ$) and high-latitude ($25^\circ < |MLAT| \leq 40^\circ$) regions are comparable to those of the near-equatorial region ($|MLAT| \leq 15^\circ$). Dayside ECH waves become stronger with increasing K_p index for $K_p < 4$, but weaken for $4 \leq K_p \leq 6$.
4. Although the occurrence rates of weak (0.01–0.1 mV/m) dayside ECH waves can be well above 25%, the occurrence rates of moderate (0.1–0.3 mV/m) and strong (> 0.3 mV/m) dayside ECH waves are nonnegligible since the peak occurrence rates can reach $\sim 8\%$ and $\sim 6\%$, respectively, thus strongly suggesting a potentially important contributor to the formation of dayside diffuse aurora, in addition to the known mechanism of dayside chorus wave scattering (Ni et al., 2014, 2016).

It is worthwhile to note that the regions of ECH waves considered in Meredith et al. (2009) focused on $-3^\circ < |MLAT| \leq 3^\circ$ and $L = 1.05-7$ and lacked the observations on the prenoon side because of the orbital limitation of CRRES. As a consequence, the preferential prenoon occurrence region reported in our study of dayside ECH waves is absent in their conclusions. On the postnoon side, the average wave amplitude of ECH waves is at the magnitude level of 10^{-2} mV/m in Meredith et al. (2009), which is larger than our results in the overlapping region. This possibly results from different calculation methods of average wave amplitude, for instance, our adoption of the data points with the ratio of peak wave intensity between $f_{ce}-2f_{ce}$ and wave intensity at f_{ce} above 5 and our computation of RMS wave amplitudes instead of arithmetic values of dayside ECH waves. However, the occurrence rates of dayside ECH waves at various wave amplitude levels are similar to their results in the overlapping region. In addition, Ni, Thorne, Horne, et al. (2011), Ni et al. (2017) used the Time History of Events and Macroscale Interactions during Substorms wave data and statistically studied the global morphology of ECH waves at $L = 5-15$ within geomagnetic latitudes $|MLAT| < 10^\circ$. Our results are also consistent with their results in that dayside ECH waves have the moderate levels of occurrence rate and

average wave amplitude especially on the prenoonside. Interestingly, our study reveals another peak occurrence region of dayside ECH waves at high latitudes owing to the broader latitudinal coverage of MMS satellites.

We can see from Figure S3 that while the majority of the data points of dayside ECH waves are distributed within $(B_{\text{local}})_{\text{MMS}}/(B_{\text{eq}})_{T04S} = 1-6$, indicating stronger magnetic field strength at off-equator latitudes, there also exists many ECH wave events that occur at $(B_{\text{local}})_{\text{MMS}}/(B_{\text{eq}})_{T04S} < 1$, especially at the latitudes of $15^\circ < |\text{MLAT}| \leq 25^\circ$. The latter strongly supports our hypothesis of dayside ECH wave occurrence at the off-equator magnetic field minimum, which requires further investigation in our future studies.

While whistler mode chorus waves are typically considered as the primary mechanism to explain the dayside diffuse aurora (Li et al., 2009; Ni et al., 2014, 2016; Shi et al., 2012), the exact role of dayside ECH waves remains unresolved because of limited information of dayside ECH wave distribution property. Thus, using the well-accumulated high-quality wave data sets from the four MMS satellites, our statistical analysis provides comprehensive and useful messages regarding the occurrence pattern of dayside ECH waves. The advantage of intensive data collection and broad latitudinal coverage of the MMS mission enables us to reveal the double peaks of dayside ECH wave occurrence zone and the considerable occurrence rates of moderate dayside ECH waves on the prenoonside of the outer magnetosphere. These observational results, together with the statistical average values of dayside ECH wave amplitude and peak wave frequency for different L shell ranges in different MLT sectors and different geomagnetic latitude intervals under different geomagnetic conditions (as tabulated in Table 1) are therefore essential to improve our current understanding of the origin of dayside diffuse aurora, the quantitative evaluation of which is however left as future investigation.

Acknowledgments

This work was supported by the NSFC grants 41574160, 41674164, 41474141, and 41204120, the Hubei Province Natural Science Excellent Youth Foundation (2016CFA044), and the Key Laboratory of Geospace Environment, Chinese Academy of Sciences, University of Science and Technology of China. D. S. acknowledges support from a Discovery Grant of the Natural Sciences and Engineering Research Council of Canada. We also thank the Magnetospheric Multiscale mission DSP and EDP Science Teams for providing the wave data and the NSSDC OMNIWeb for the use of solar wind and geomagnetic index data. All MMS data used are available at (<https://lasp.colorado.edu/mms/sdc/public/about/browse-wrapper/>). Solar wind data and geomagnetic indices are available in OMNIWeb (<http://omniweb.gsfc.nasa.gov/>).

References

- Ashour-Abdalla, M., & Kennel, C. F. (1978). Nonconvective and convective electron cyclotron harmonic instabilities. *Journal of Geophysical Research*, 83, 1531–1543. <https://doi.org/10.1029/JA083iA04p01531>
- Belmont, G., Fontaine, D., & Canu, P. (1983). Are equatorial electron cyclotron waves responsible for diffuse auroral electron precipitation? *Journal of Geophysical Research*, 88, 9163–9170. <https://doi.org/10.1029/JA088iA11p09163>
- Burch, J. L., Moore, T. E., Torbert, R. B., & Giles, B. L. (2016). Magnetospheric multiscale overview and science objectives. *Space Science Reviews*, 199(1–4), 5–21. <https://doi.org/10.1007/s11214-015-0164-9>
- Burch, J. L., & Torbert, R. B. (2016). Preface. *Space Science Reviews*, 199(1–4), 1–3. <https://doi.org/10.1007/s11214-015-0153-z>
- Case, N. A., & Wild, J. A. (2013). The location of the Earth's magnetopause: A comparison of modeled position and in situ Cluster data. *Journal of Geophysical Research: Space Physics*, 118, 6127–6135. <https://doi.org/10.1002/jgra.50572>
- Ergun, R. E., Tucker, S., Westfall, J., Goodrich, K. A., Malaspina, D. M., Summers, D., Wallace, J., et al. (2016). The axial double probe and fields signal processing for the MMS mission. *Space Science Reviews*, 199(1–4), 167–188. <https://doi.org/10.1007/s11214-014-0115-x>
- Fuselier, S. A., Lewis, W. S., Schiff, C., Ergun, R., Burch, J. L., Petrinec, S. M., & Trattner, K. J. (2016). Magnetospheric multiscale science Mission profile and operations. *Space Science Reviews*, 199(1–4), 77–103. <https://doi.org/10.1007/s11214-014-0087-x>
- Gurnett, D. A., & Bhattacharjee, A. (2005). Introduction to plasma physics: With space and laboratory applications (pp. 341–390). Cambridge, UK: Cambridge University Press.
- Han, D. S., Li, J. X., Nishimura, Y., Lyons, L. R., Bortnik, J., Zhou, M., Liu, J. J., et al. (2017). Coordinated observations of two types of diffuse auroras near magnetic local noon by Magnetospheric multiscale Mission and ground all-sky camera. *Geophysical Research Letters*, 44, 8130–8139. <https://doi.org/10.1002/2017GL074447>
- Horne, R. B. (1989). Path-integrated growth of electrostatic waves: The generation of terrestrial myriametric radiation. *Journal of Geophysical Research*, 94, 8895–8909. <https://doi.org/10.1029/JA094iA07p08895>
- Horne, R. B., Thorne, R. M., Meredith, N. P., & Anderson, R. R. (2003). Diffuse auroral electron scattering by electron cyclotron harmonic and whistler mode waves during an isolated substorm. *Journal of Geophysical Research*, 108(A7), 1029. <https://doi.org/10.1029/2002JA009736>
- Kennel, C. F., Scarf, F. L., Fredricks, R. W., Mcghee, J. H., & Coroniti, F. V. (1970). VLF electric field observations in the inner magnetosphere. *Journal of Geophysical Research*, 75, 6136–6152. <https://doi.org/10.1029/JA075i031p06136>
- Li, J., Bortnik, J., An, X., Li, W., Russell, C. T., Zhou, M., Berchem, J., et al. (2018). Local excitation of whistler mode waves and associated Langmuir waves at dayside reconnection regions. *Geophysical Research Letters*, 45, 8793–8802. <https://doi.org/10.1029/2018GL078287>
- Li, W., Bortnik, J., Thorne, R. M., & Angelopoulos, V. (2011). Global distribution of wave amplitudes and wave normal angles of chorus waves using THEMIS wave observations. *Journal of Geophysical Research*, 116, A12205. <https://doi.org/10.1029/2011JA017035>
- Li, W., Thorne, R. M., Angelopoulos, V., Bortnik, J., Cully, C. M., Ni, B., LeContel, O., et al. (2009). Global distribution of whistler-mode chorus waves observed on the THEMIS spacecraft. *Geophysical Research Letters*, 36, L09104. <https://doi.org/10.1029/2009GL037595>
- Liang, J., Ni, B., Spanswick, E., Kubyshkina, M., Donovan, E. F., Uritsky, V. M., Thorne, R. M., et al. (2011). Fast earthward flows, electron cyclotron harmonic waves, and diffuse auroras: Conjunctive observations and a synthesized scenario. *Journal of Geophysical Research*, 116, A12220. <https://doi.org/10.1029/2011JA017094>
- Lindqvist, P. A., Olsson, G., Torbert, R. B., King, B., Granoff, M., Rau, D., Torbert, R. B., et al. (2016). The spin-plane double probe electric field instrument for MMS. *Space Science Reviews*, 199(1–4), 137–165. <https://doi.org/10.1007/s11214-014-0116-9>
- Lui, A. T. Y., Venkatesan, D., Anger, C. D., Akasofu, S.-I., Heikkila, W. J., Winningham, J. D., & Burrows, J. R. (1977). Simultaneous observations of particle precipitations and auroral emissions by the Isis 2 satellite in the 19–24 MLT sector. *Journal of Geophysical Research*, 82, 2210–2226. <https://doi.org/10.1029/JA082i016p02210>
- Meng, C.-I., Mauk, B., & McIlwain, C. E. (1979). Electron precipitation of evening diffuse aurora and its conjugate electron fluxes near the magnetospheric equator. *Journal of Geophysical Research*, 84, 2545–2558. <https://doi.org/10.1029/JA084iA06p02545>

- Meredith, N. P., Horne, R. B., Thorne, R. M., & Anderson, R. R. (2009). Survey of upper band chorus and ECH waves: Implications for the diffuse aurora. *Journal of Geophysical Research*, 114, A07218. <https://doi.org/10.1029/2009JA014230>
- Newell, P. T., Sotirelis, T., & Wing, S. (2009). Diffuse, monoenergetic, and broadband aurora: The global precipitation budget. *Journal of Geophysical Research*, 114, A09207. <https://doi.org/10.1029/2009JA014326>
- Ni, B., Bortnik, J., Nishimura, Y., Thorne, R. M., Li, W., Angelopoulos, V., Ebihara, Y., et al. (2014). Chorus wave scattering responsible for the Earth's dayside diffuse auroral precipitation: A detailed case study. *Journal of Geophysical Research: Space Physics*, 119, 897–908. <https://doi.org/10.1002/2013JA019507>
- Ni, B., Gu, X., Fu, S., Xiang, Z., & Lou, Y. (2017). A statistical survey of electrostatic electron cyclotron harmonic waves based on THEMIS FFF wave data. *Journal of Geophysical Research: Space Physics*, 122, 3342–3353. <https://doi.org/10.1002/2016JA023433>
- Ni, B., Liang, J., Thorne, R. M., Angelopoulos, V., Horne, R. B., Kubyshkina, M., Spanswick, E., et al. (2012). Efficient diffuse auroral electron scattering by electrostatic electron cyclotron harmonic waves in the outer magnetosphere: A detailed case study. *Journal of Geophysical Research*, 117, A01218. <https://doi.org/10.1029/2011JA017095>
- Ni, B., & Thorne, R. (2012). Recent advances in understanding the diffuse auroral precipitation: The role of resonant wave-particle interactions. In D. Summers, I. R. Mann, D. N. Baker, & M. Schulz (Eds.), *Dynamics of the Earth's Radiation Belts and Inner Magnetosphere, Geophysical Monograph Series* (Vol. 199, pp. 291–302). Washington, DC: American Geophysical Union. <https://doi.org/10.1029/2012GM001337>
- Ni, B., Thorne, R., Liang, J., Angelopoulos, V., Cully, C., Li, W., Zhang, X., et al. (2011). Global distribution of electrostatic electron cyclotron harmonic waves observed on THEMIS. *Geophysical Research Letters*, 38, L17105. <https://doi.org/10.1029/2011GL048793>
- Ni, B., Thorne, R. M., Horne, R. B., Meredith, N. P., Shprits, Y. Y., Chen, L., & Li, W. (2011). Resonant scattering of plasma sheet electrons leading to diffuse auroral precipitation: 1. Evaluation for electrostatic electron cyclotron harmonic waves. *Journal of Geophysical Research*, 116, A04218. <https://doi.org/10.1029/2010JA016232>
- Ni, B., Thorne, R. M., Meredith, N. P., Horne, R. B., & Shprits, Y. Y. (2011). Resonant scattering of plasma sheet electrons leading to diffuse auroral precipitation: 2. Evaluation for whistler mode chorus waves. *Journal of Geophysical Research*, 116, A04219. <https://doi.org/10.1029/2010JA016233>
- Ni, B., Thorne, R. M., Shprits, Y. Y., & Bortnik, J. (2008). Resonant scattering of plasma sheet electrons by whistler-mode chorus: Contributions to diffuse auroral precipitation. *Geophysical Research Letters*, 35, L11106. <https://doi.org/10.1029/2008GL034032>
- Ni, B., Thorne, R. M., Zhang, X., Bortnik, J., Pu, Z., Xie, L., Hu, Z. J., et al. (2016). Origins of the Earth's diffuse auroral precipitation. *Space Science Reviews*, 200(1–4), 205–259. <https://doi.org/10.1007/s11214-016-0234-7>
- Roeder, J. L., & Koons, H. C. (1989). A survey of electron cyclotron waves in the magnetosphere and the diffuse auroral precipitation. *Journal of Geophysical Research*, 94, 2529–2541. <https://doi.org/10.1029/JA094IA03p02529>
- Russell, C. T., Anderson, B. J., Baumjohann, W., Bromund, K. R., Dearborn, D., Fischer, D., et al. (2016). The magnetospheric multiscale magnetometers. *Space Science Reviews*, 199(1–4), 189–256. <https://doi.org/10.1007/s11214-014-0057-3>
- Shabansky, V. P. (1971). Some processes in the magnetosphere. *Space Science Reviews*, 12, 299–418. <https://doi.org/10.1007/BF00165511>
- Shi, R., Han, D., Ni, B., Hu, Z.-J., Zhou, C., & Gu, X. (2012). Intensification of dayside diffuse auroral precipitation: Contribution of dayside whistler-mode chorus waves in realistic magnetic fields. *Annales Geophysicae*, 30, 1297–1307. <https://doi.org/10.5194/angeo-30-1297-2012>
- Tao, X., Thorne, R. M., Li, W., Ni, B., Meredith, N. P., & Horne, R. B. (2011). Evolution of electron pitch angle distributions following injection from the plasma sheet. *Journal of Geophysical Research*, 116, A04229. <https://doi.org/10.1029/2010JA016245>
- Thorne, R. M., Ni, B., Tao, X., Horne, R. B., & Meredith, N. P. (2010). Scattering by chorus waves as the dominant cause of diffuse auroral precipitation. *Nature*, 467(7318), 943–946. <https://doi.org/10.1038/nature09467>
- Torbert, R. B., Russell, C. T., Magnes, W., Ergun, R. E., Lindqvist, P. A., LeContel, O., Vaith, H., et al. (2016). The FIELDS instrument suite on MMS: Scientific objectives, measurements, and data products. *Space Science Reviews*, 199(1–4), 105–135. <https://doi.org/10.1007/s11214-014-0109-8>
- Tsyganenko, N. A., & Sitnov, M. I. (2005). Modeling the dynamics of the inner magnetosphere during strong geomagnetic storms. *Journal of Geophysical Research*, 110, A03208. <https://doi.org/10.1029/2004JA010798>
- Wilder, F. D., Ergun, R. E., Goodrich, K. A., Goldman, M. V., Newman, D. L., Malaspina, D. M., Jaynes, A. N., et al. (2016). Observations of whistler mode waves with nonlinear parallel electric fields near the dayside magnetic reconnection separatrix by the Magnetospheric multiscale mission. *Geophysical Research Letters*, 43, 5909–5917. <https://doi.org/10.1002/2016GL069473>
- Zhang, X.-J., & Angelopoulos, V. (2014). On the relationship of electrostatic cyclotron harmonic emissions with electron injections and dipolarization fronts. *Journal of Geophysical Research: Space Physics*, 119, 2536–2549. <https://doi.org/10.1002/2013JA019540>